

Hematite-rich concretions from Mesoproterozoic Vindhyan sandstone in northern India: a terrestrial Martian ‘blueberries’ analogue with a difference

Jayanta K. Pati^{1,*}, Kamal L. Pruseth², Rajat S. Chatterjee³, Suresh C. Patel⁴, Kuldeep Prakash¹, Munmun Chakarvorty¹, Ram P. Singh¹, Rabi Bhushan¹, Vivek P. Malviya¹, Richa Sharma³ and Prashanta K. Champati Ray³

¹Department of Earth and Planetary Sciences, University of Allahabad, Allahabad 211 002, India

²Department of Geology and Geophysics, Indian Institute of Technology, Kharagpur 721 302, India

³Geoscience Division, Indian Institute of Remote Sensing, Dehradun 248 001, India

⁴Department of Earth Sciences, Indian Institute of Technology, Powai, Mumbai 400 076, India

We report here hematite-rich concretions observed in the sandstone of the Mesoproterozoic Vindhyan Supergroup of rocks occurring in parts of Bihariya, Uttar Pradesh, northern India. These concretions are similar to ‘blueberries’ from Mars and their terrestrial analogues reported from the Jurassic Navajo Sandstone in Utah, USA. The presence of diagenetically formed hematite concretions gave the first confirmation of the presence of liquid water in the red planet in the past. We report here the detailed morphology, petrography, mineral chemistry, magnetic susceptibility characteristics and spectral radiometric data of hematite-rich concretions observed in the Vindhyan sandstone. These are compared with ‘blueberries’ from Mars and other similar terrestrial analogues reported from different parts of the world. In spite of similarities, these hematite-rich concretions are strikingly distinct in having a nucleus and alternate iron-rich and iron-poor rims unlike other global occurrences. In addition, we document here outcrop scale evidence of possible fluid pathways considered responsible for the development of the concretions.

Keywords: Concretions, diagenesis, hematite, sandstone, terrestrial analogues.

SPHERICAL hematite concretions (<0.5 cm in diameter) were first observed on a 22 m diameter Meridiani crater rim by the rover’s camera five days after Mars Opportunity landed on the Martian surface on 25 January 2004 (ref. 1). The lead rover scientist Steve Squyres named the millimetre sized spheres embedded in a light-coloured rock outcrop as ‘blueberries’ (Figure 1 *a*). Since hematite mostly forms in presence of water, these blueberries suggest that liquid water was once present on Mars. The

terrestrial analogue of Martian blueberries (MB) was first reported from the Jurassic Navajo Sandstone, Utah, USA² and was suggested to have formed due to complex diagenetic concretion-forming processes^{3,4}. Despite the similarities, the nearly pure hematite-bearing MB are different from the Utah concretions (UC) (Figure 1 *b*), which are typical arenites with hematite cement. MB are believed to have formed from acidic standing water or groundwater, whereas UC have formed by the interaction of hydrocarbon-rich briny fluids with oxygen-rich groundwater. Numerical simulations and experimental studies have shown that the concretions form around a nucleation centre when shallow freshwater interacts with iron-charged deeper and reduced formation water⁵. Other reported terrestrial analogues include hematite concretions occurring within evaporite–siliciclastic sequences of Permian age in the central United States⁶, and of modern age in Western Australia^{7,8}. Hematite spherules are found within sulphate-rich rocks on Mauna Kea volcano, Hawaii⁹.

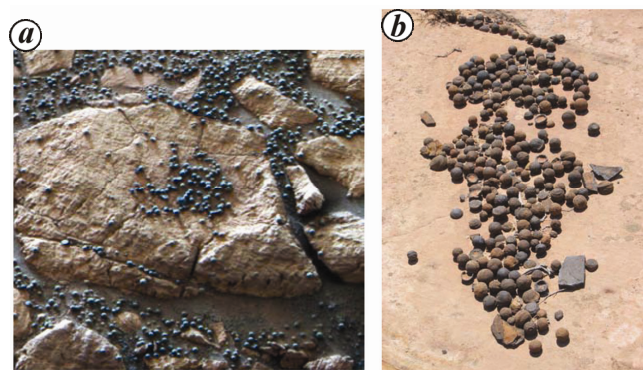


Figure 1. *a*, Martian blueberries photograph taken from Mars Opportunity rover (source: <http://mars.gov>). *b*, Closeup of hematite concretions from Grand Staircase, Escalante National Monument, Utah, USA (Source: <http://unews.utah.edu/>; Photo credit: Brenda Beitler.)

*For correspondence. (e-mail: jkpati@gmail.com)

However, Glotch *et al.*¹⁰ proposed the possibility that MB could have formed as impact melt spherules or as volcanic lapilli. A recent study shows that the hematite-rich concretions are actively forming in shallow subsurface sediments in Lake Brown, Western Australia, as early diagenetic products in acid and saline conditions¹¹, contrary to the earlier held view that hematite concretions in the Burns Formation on Mars have formed as late-stage diagenetic products. Nevertheless, such concretions on Earth are considered to be useful in deciphering the sediment burial history, physico-chemical conditions of depositional environments, palaeobiology and palaeoclimate^{12,13}. The mobility of iron is essential for the formation of hematite concretions in sedimentary rocks and this requires a change in Eh and pH of the fluid phase occurring within the intergranular pore spaces of the sediments with or without microbial activity¹¹. It is extremely

significant to further study the terrestrial analogues, since NASA's a sample return mission to Mars is in the offing. The present study reports hematite-rich concretions in quartz arenites (Dhandraul Sandstone, Kaimur Group, Vindhyan Supergroup) of Mesoproterozoic age from a location 300 m SE of Bihariya village (25°13'54.6"N; 81°32'27.3"E), Allahabad district, Uttar Pradesh, India (Figure 2 a–c). These concretions (Figure 3 a–d) are quite similar to the terrestrial analogues of MB reported from the Jurassic Navajo Sandstone of Jurassic age². The present instance of blueberries analogue is from the much older lithology (Mesoproterozoic age) reported till date. The Rb–Sr isochron data of intrusive kimberlites¹⁴ suggests the age sandstone of Kaimur Group to be >1067 Ma. Here we discuss the morphology, petrography, mineral chemistry, X-ray diffraction characteristics, bulk-rock magnetic susceptibility and spectro-radiometric data of the hematite-rich concretions from Bihariya. The spectral signatures of these concretions are compared with those from other terrestrial Martian analogues and data available on MB.

Geology of the study area

The hematite-rich concretions of the Bihariya area are embedded within friable quartz arenites (Figure 3 a and d) which are well known for high-quality silica sand¹⁵. Stratigraphically, these quartz arenites are grouped under the Dhandraul Sandstone of the Kaimur Group (Vindhyan Supergroup) of Mesoproterozoic age. The quartz arenite varies in thickness from 30 to 150 m and is suggested to have formed under multiple fluctuating depositional environments like fluvial, aeolian and near shore¹⁶.

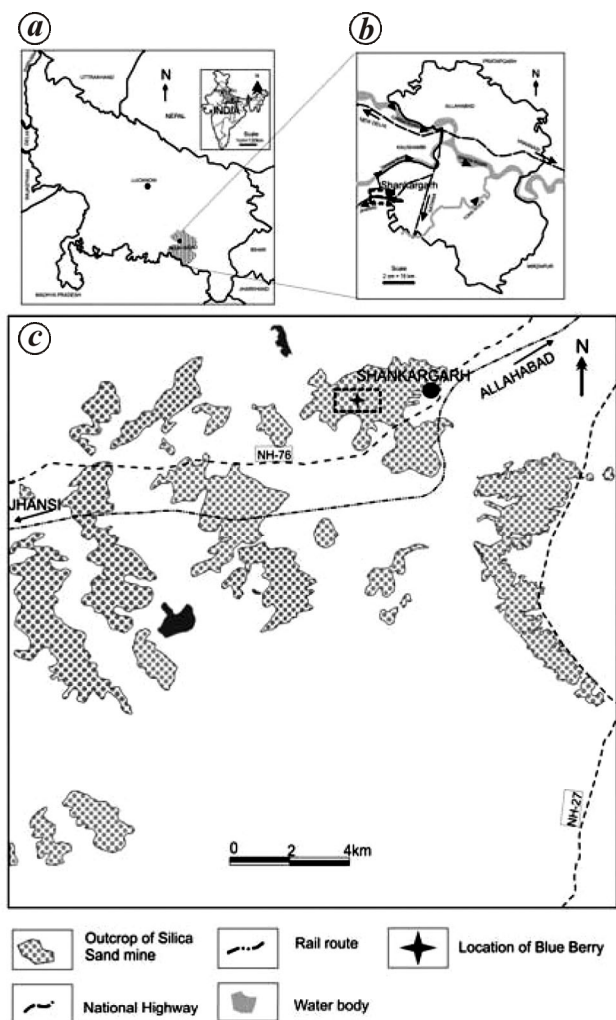


Figure 2. Map of study area with hematite-rich concretions in quartz arenites (Dhandraul Sandstone, Kaimur Group, Vindhyan Supergroup) of Mesoproterozoic age from a location 300 m SE of Bihariya village (25°13'54.6"N; 81°32'27.3"E), Allahabad district, Uttar Pradesh, India.

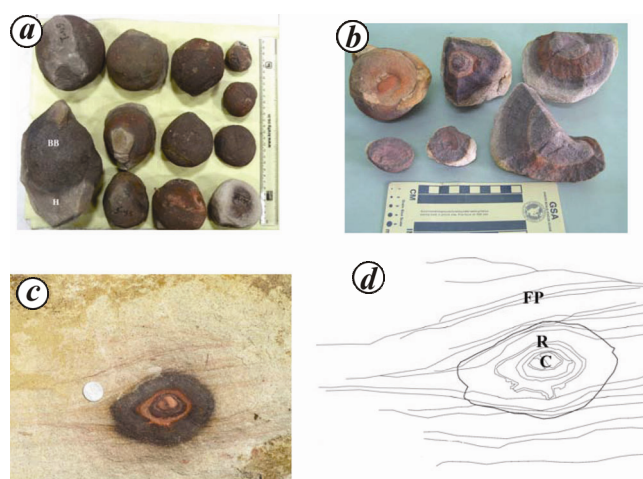


Figure 3. a, Hematite-rich concretions of the Bihariya area embedded within friable quartz arenites. b, Cross-section of some hematite-rich concretions. c, d, The fluid pathways cut across the concretionary body. Diameter of the coin is 2.5 cm. BB, Blueberries, H, Host rock (arenite), C, Core, R, Rim, and FP, Fluid pathways.

The quartz arenites are light grey to pale yellowish-brown in colour, moderately to thickly bedded, and contain different sedimentary structures such as planar bedding, small and large-scale cross beddings and ripple marks. The top of the formation is locally capped by ferricrete in the study area. Pervasive sub-vertical, NNW-trending fractures of tectonic origin dissect the sub-horizontal bedding and local scale slump structures observed in the area¹⁷. The quartz arenites are well exposed in more than 122 silica sand mining sites, which are spread over an area of ~80 sq. km (Figure 2). The present study is mainly confined to Bihariya, where hematite concretions are common. The concretions designated as Vindhyan hematite concretions (VHC) are easily separable from host friable quartz arenites and all 29 samples of such concretions have been collected from the silica sand mines occurring in this area.

Megascopic characterization of hematite concretions

The VHC are mainly spherical to elliptical in shape. Their long axes measure between 5.1 and 12.5 cm compared to short axes lengths varying from 3.4 to

10.4 cm (Table 1). The Waddell's sphericity index has been measured for 25 out of the 29 concretions (Table 1) and it ranges between 0.78 and 0.98. For the remaining four concretions, there is uncertainty in measuring the third dimension. The concretions show discrete multiple coalescence and co-joined forms. They are bluish-grey to reddish-brown in colour (Figure 3 a). The VHC show a core with nucleus (single or multiple) surrounded by multiple rims (Figure 3 b). Up to 12 rims have been observed in these concretions. The thickness of the individual rim is variable (0.1–5 cm). The rims show different shades of colour and they can be easily differentiated (Figure 3 b). The light layers are mostly buff-coloured and occur close to the cores (Figure 3 b). The shape of the core is seldom circular and varies from near circular, elliptical to dumb-bell shaped. In 70% of the concretions, the core consists of a nucleus, which is angular to elliptical in shape and is invariably composed of kaolinite (Figure 3 b). An *in situ* outcrop occurrence of an elliptical hematite-rich concretion with distinct core, multiple rims of varying colours and thicknesses with a number of brownish-red laminae indicating the possible fluid pathways is shown in Figure 3 c (25°13'52.2"N; 81°32'27.8"E). The layers are seen to warp around the concretions and follow curved traces of the concretion both inside as well as outside similar to layering geometries reported earlier¹² in concretionary structures. In some places the 'fluid pathways'¹² cut across the layerings (Figure 3 c and d).

Table 1. Dimensions of hematite concretions from Bihariya area, Allahabad district, Uttar Pradesh, India

Sample no.	Long axis (cm)	Intermediate axis (cm)	Short axis (cm)	Waddell's sphericity
SG-1	11.75	11.6	8.14	0.88
SG-2	9.15	8.52	8.62	0.95
SG-3	8.8	8.7	8	0.96
SG-4	8.8	8.3	8.2	0.95
SG-5	9.1	7.8	7.1	0.87
SG-6	9.6	8.1	6.3	0.82
SG-7	6.1	5.9	5.7	0.96
SG-8	6.4	5.3	5.1	0.87
SG-9	7.3	5.3	4.8	0.78
SG10	7.6	N.D.	7.1	–
SG-11	6.5	N.D.	5.6	–
SG-12	7.7	N.D.	6.1	–
SG-13	8.3	8.1	7.1	0.94
SG-14	9.3	8.9	8.4	0.95
SG-15	7.9	7.7	7.7	0.98
SG-16	7.3	7.1	6.4	0.94
SG-17	6.1	5.8	5.3	0.93
SG-18	8.4	7.7	6.4	0.88
SG-19	6.4	6.1	5.5	0.93
SG-20	5.8	5.7	4.3	0.89
SG-21	7.4	7.1	6.3	0.93
SG-22	4.9	4.5	4.3	0.93
SG-23	5.4	5.3	4.7	0.95
SG-24	8.2	8.1	7.9	0.98
SG-25	12.5	11.6	10.4	0.91
SG-27	5.1	4.9	4.6	0.95
SG-28	12.1	10.6	9.6	0.88
SG-29	5.1	4.9	3.9	0.90

N.D., Not determined.

Petrography and mineralogy

Detailed petrographic study of 21 thin-sections shows that the VHC are predominantly made up of framework quartz grains (Figure 4 a) with a small amount of other mineral grains and lithic fragments (Figure 4 b and c) embedded in ferruginous cement (hematite and goethite) (Figure 4 d and e). The long and short axes of 423 mineral grains have been measured in thin sections of the concretions. The shape of quartz grains varies from subangular to subrounded or rounded, and ranges in size from 0.03 to 2.18 mm with an average of 0.2 mm. The ratio of mineral to lithic grains is 7 : 1 in light coloured layers. The lithic grains mostly show rounded shape, and are 0.07 to 0.4 mm in size with an average size of 0.16 mm. The grain-to-cement ratio varies between 60 : 40 and 80 : 20. Some of the quartz grains show undulose extinction and sub-grain development with serrated grain boundaries (Figure 4 c). Some other quartz grains show Boehm and bent twin lamellae. However, the majority of the quartz grains are strain-free. The grains of strained quartz and tourmaline are rounded. Grains of glauconite, tourmaline, zircon, apatite and rutile occur in traces (Figure 4 b–e). The diagenetically formed phases include hematite, goethite and clay minerals (kaolinite

and illite). Goethite occurs as ferruginous cement within the intergranular space of the concretions (Figure 4 *b* and *d*). Quartz grains show floating-, point-, long-, sutured- and concave-convex contacts. Some pressure solution contacts and deformed mica flakes between quartz grains are also observed (Figure 4 *f*). The dark-coloured rims of the concretions have higher proportions of ferruginous cement while clay cement is characteristic of the light coloured rims. Furthermore, different dark and light coloured rims have variable contents of cement relative to framework fraction. Lithologically, the VHC can be classified as ferruginous arenite, whereas the host rock is a moderately sorted arenite.

The X-ray diffraction patterns obtained using a Philips XRD (X'Pert High Score) for 10 representative concretions show the presence of quartz, hematite, muscovite, montmorillonite, goethite and kaolinite (Figure 5). Quartz has a very strong reflection at $26.63^\circ 2\theta$ (Cu $K\alpha$) with d-spacing of 3.34 Å. Hematite and goethite are identified based on their characteristic d-spacings of 2.7 and 4.2 Å respectively. Kaolinite has its maximum intensity peak at

$12.3^\circ 2\theta$ with d-spacing of 7.2 Å. Chemical compositions of the mineral phases other than tourmaline and apatite present in the concretions have been determined by Cameca SX-100 electron microprobe at IIT, Roorkee (Table 3). Quartz is nearly pure ($\text{SiO}_2 = 92.42\text{--}99.19$ wt%) with traces of Fe_2O_3 (0.32–0.69) and TiO_2 (0–0.02). Other minerals analysed include hematite ($\text{Fe}_2\text{O}_3\text{T}$: 147.94.11–96.27 wt%), goethite ($\text{Fe}_2\text{O}_3\text{T}$: 79.52–79.86 wt%), kaolinite (Al_2O_3 : 37.91 wt%), glauconite (K_2O : 4.21 wt%; $\text{Fe}_2\text{O}_3\text{T}$: 17.1 wt%), K-feldspar (K_2O : 14.86 wt%; SiO_2 : 64.19 wt%) and brookite (TiO_2 : 95.95–96.15 wt%).

Magnetic susceptibility measurements

The concretions are sliced into thin slabs. The core, rim and host rock portions were cut from the slabs using a hand-held electric saw. The individual samples are weighed using a Mettler Toledo electronic balance (Model No. AB104, Germany). The magnetic susceptibility measurements of the samples comprising core, rim and host rocks were made (in SI units) using a dual frequency (0.47 and 4.7 kHz) magnetic susceptibility meter (MS2B; Bartington, UK) (Table 3). The two samples (SG-26 and SG-28) having core, rim and host-rock portions show varied mass magnetic susceptibility values ($0.70\text{--}3.49 \times 10^{-8} \text{ m}^3 \text{ kg}^{-1}$) at low frequency. The host arenites (0.70 and $0.83 \times 10^{-8} \text{ m}^3 \text{ kg}^{-1}$) are poor in ferri-magnetic minerals (hematite and goethite) compared to the outer rims (3.42 and $3.43 \times 10^{-8} \text{ m}^3 \text{ kg}^{-1}$), inner rims (3.42 and $3.49 \times 10^{-8} \text{ m}^3 \text{ kg}^{-1}$) and core portions (1.62 and $2.72 \times 10^{-8} \text{ m}^3 \text{ kg}^{-1}$). The SG-26 core shows relatively higher magnetic susceptibility value ($2.72 \times 10^{-8} \text{ m}^3 \text{ kg}^{-1}$) compared to the core of SG-28 ($1.62 \times 10^{-8} \text{ m}^3 \text{ kg}^{-1}$) possibly due to the presence of clay-rich diamagnetic minerals ($-0.58\text{--}0.48 \times 10^{-8} \text{ m}^3 \text{ kg}^{-1}$) present in the sample.

Spectro-radiometric measurements and analysis

The spectro-radiometric measurements of the core portion and light-coloured nucleus of sliced concretion samples (SR-29 and BB-2) were made (Figure 6) using a hand-held spectroradiometer (ASD FieldSpec 4 Hi-Res spectroradiometer, Analytical Spectral Devices, Inc.) between wavelength ranges 350 and 2500 nm. Figure 6 shows the spectrum for SR-29. There are three spectrometers in the instrument: one in the VNIR (350–1050 nm) region and two are in the SWIR (1000–2500 nm) regions, namely SWIR1 (900–1850 nm) and SWIR2 (1700–2500 nm). The instrument provides the highest spectral resolution (8 nm) available in a portable field spectroradiometer with vastly improved signal throughput (2X radiometric performances in SWIR-1 and SWIR-2) and signal-to-noise ratio over previous ASD field spectrometers. Spectral measurements of the

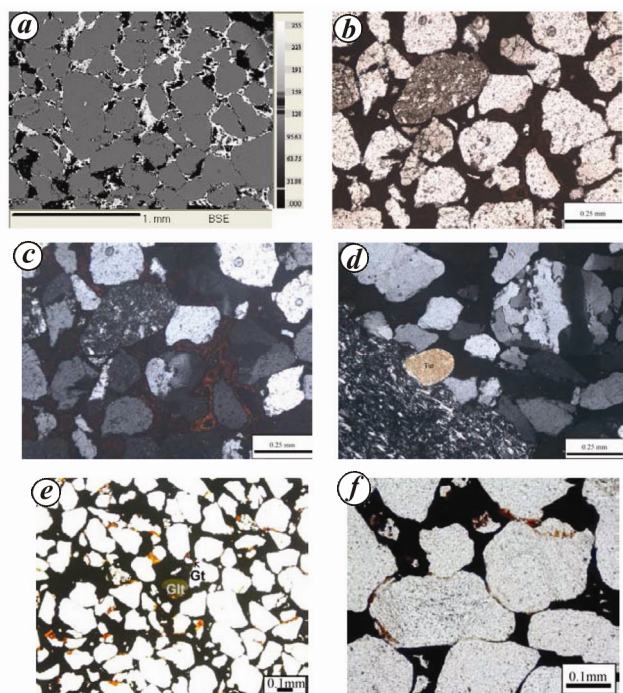


Figure 4. *a*, BSE-SEM image showing hematite-rich concretions comprising quartz grains of varied size and shape within ferruginous cement. *b*, Plane-polarized view of thin section showing lithic and mineral grains (mostly quartz) in a ferruginous cement. *c*, Crossed polar photomicrograph showing the association of goethite mineral with ferruginous minerals occurring within the framework quartz grains. *d*, Crossed polar view showing the association of clay-rich lithic grains and mineral grains (quartz, tourmaline, sericite and opaque phases) in a ferruginous cement. *e*, Glauconite (Glt) at the centre and goethite (Gt) in a quartz arenite with framework grains exhibiting varied size and shape in plane polarized view. *f*, Quartz grains in plane polarized light show floating, line, sutured, concave-convex and pressure-solution contacts.

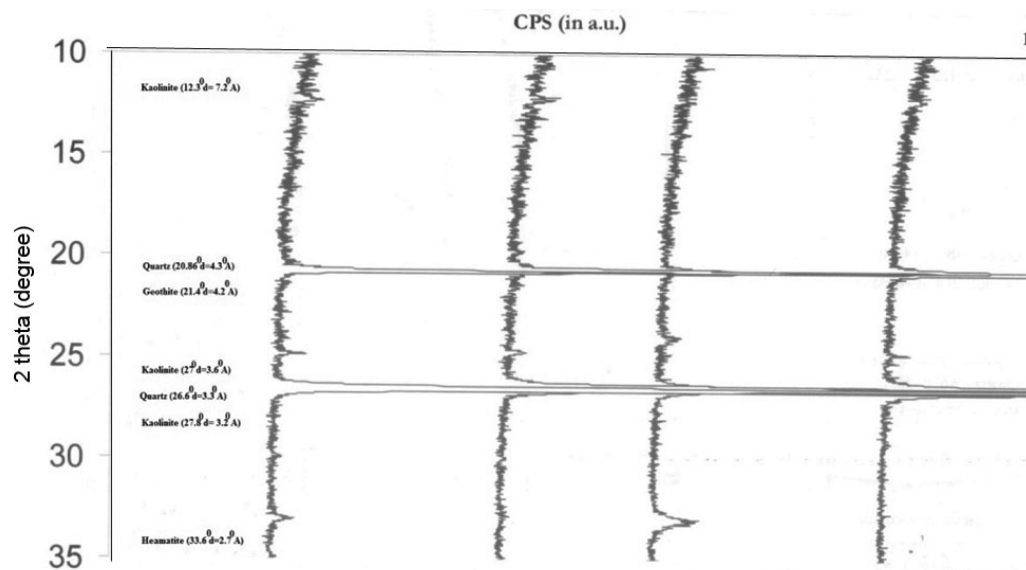


Figure 5. XRD patterns of hematite concretions showing the presence of different minerals.

Table 2. Electron probe micro analysis of selected phases occurring within concretion layers

	Quartz	Quartz	Quartz	Hema- tite	Hema- tite	Hema- tite	Goethite	Goethite	Goethite	Broo- kite	Broo- kite	K- feldspar	Glau	Kaoli- nite
Na ₂ O	0	0.03	0	0.07	0.07	0.56	0.13	0.15	0.15	0	0.02	1.08	0.59	0.04
MgO	0	0.01	0	0.01	0.05	0.06	0.03	0.06	0.06	0.02	0	0	10.32	0.02
Al ₂ O ₃	0.02	0.05	0	0.41	0.59	0.35	0.32	1.72	1.72	0.19	0.22	18.79	17.53	37.91
SiO ₂	99.03	99.19	99.04	2.2	2.3	2.49	4.46	4.03	4.03	0.03	0.05	64.19	34.53	46.87
K ₂ O	0.01	0	0.01	0.02	0.03	0.08	0.01	0.02	0.02	0.01	0.01	14.86	4.21	0.28
CaO	0	0.01	0.01	0.07	0.09	0.15	0.09	0.09	0.09	0.07	0.08	0	2.15	0.04
TiO ₂	0	0.02	0	0.05	0	0	0.01	0.07	0.07	95.95	96.15	0	1.12	0.02
MnO	0.01	0.02	0.02	0.04	0	0	0.05	0.05	0.05	0	0	0.01	0.13	0.02
TFe ₂ O ₃	0.69	0.33	0.32	96.27	95.37	94.11	79.52	79.86	79.86	0.81	0.58	0.06	17.1	0.24
NiO	0.02	0.01	0.01	0.01	0.02	0.01	0.02	0.02	0.02	0.04	0	0.01	0	0.04
Total	99.74	99.67	99.33	99.06	98.48	97.81	84.64	86.09	86.09	96.64	96.67	98.96	87.68	85.48

Table 3. Magnetic susceptibility measurements of portions of hematite concretions and host rocks using a dual frequency Magnetic Susceptibility Meter (MS2B, Bartington, UK)

Sample no.	Sample details	Magnetic susceptibility			
		Low frequency		High frequency	
		Mean (10)	SD	Mean (10)	SD
SG-26	Core	2.72	0.1	2.61	0.12
SG-26	Inner rim	3.42	0.35	2.69	0.07
SG-26	Outer rim	3.42	0.25	2.68	0.13
SG-26	Host	0.70	0.16	0.23	0.11
SG-28	Core	1.62	0.11	0.74	0.33
SG-28	Inner rim	3.49	0.22	2.65	0.12
SG-28	Outer rim	3.43	0.23	2.71	0.14
SG-28	Host	0.83	0.17	0.53	0.21

samples (SR-29 and BB-2) were made over the entire spectral range (350–2500 nm) of the instrument covered by VNIR, SWIR1 and SWIR2 spectrometers. It may be

noted here that the three spectrometer arrays warm up at different rates, which may result in subtle spectral offsets in the overlap regions.

Spectral plot of the core (BB-2) typically indicates the presence of hematite in the sample with the presence of a prominent absorption peak at around 700 nm. The presence of goethite can be confirmed in both the samples by the presence of typical absorption peaks at around 1400 and 1900 nm. Similar observations have been noted on Martian simulants¹⁸. Besides iron oxide and iron hydroxide, the presence of clay minerals such as kaolinite and illite may be confirmed by the absorption peaks at around 2200 and 2400 nm respectively. The presence of quartz is verified by the absorption peak at 1900 nm. Subtle spectral offsets were observed at 1050 and 1800 nm (overlapping regions of VNIR versus SWIR-1, and SWIR-1 versus SWIR-2) in both the samples. The presence of a mixture of goethite and hematite in our samples predicts a similar composition for the bright areas on Mars. The spectral data of the samples, which appear to be a mixture

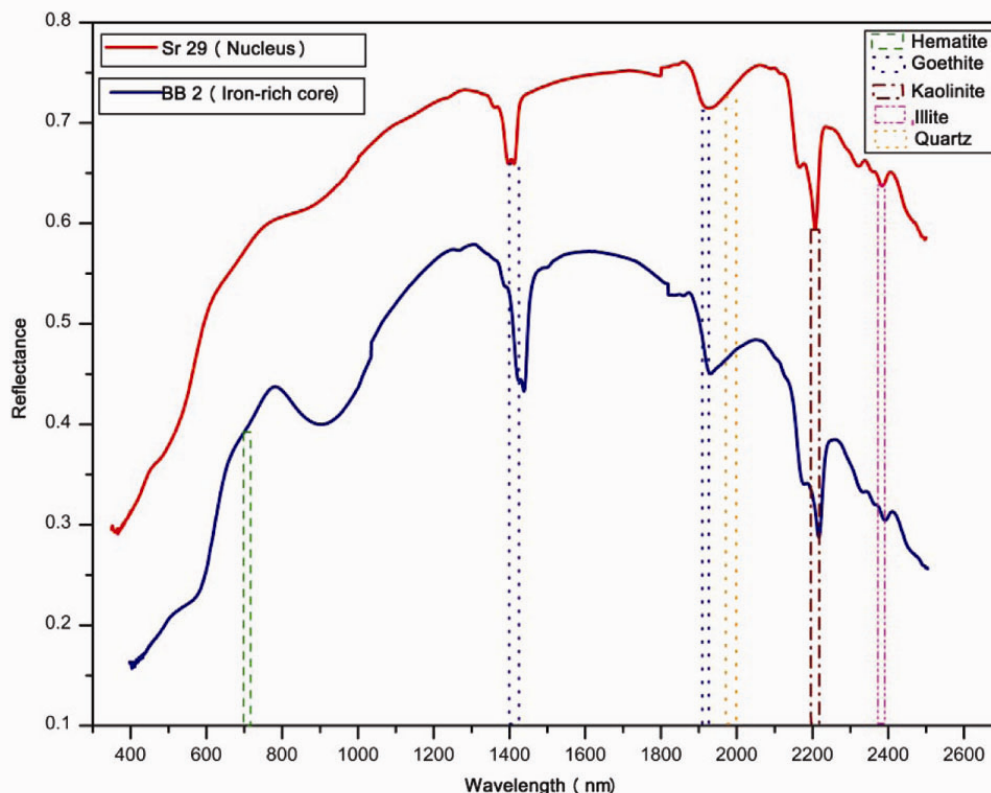


Figure 6. Spectro-radiometric measurements of core portion (BB-2) and light-coloured nucleus (Sr-29) of a sliced hematite concretion.

of goethite (hydrated iron oxide) and hematite (iron oxide), agrees, in general, in the 800–1100 nm regions with the spectrum of the bright areas of Mars¹⁹.

Results and discussion

The VHC are morphologically similar to UC and MB with certain differences. MB have uniform shape (nearly spherical having average aspect ratio of 1.06) compared to spherical to elliptical shapes observed in case of VHC with aspect ratio varying between 1.03 and 1.52 (average = 1.21). Co-joined forms are noted in the VHC and are also reported from MB and UC. The VHC possess a nucleus, alternate iron-rich and iron-poor rims, unlike MB which have uniform hematite distribution without displaying any concentric shells. Predominantly UC shows core and rim structure. The host rocks in case of VHC are fine-to coarse-grained (0.03–2.12 mm) arenites with hematite (\pm goethite) concretion cements in case of VHC compared to fine-grained sedimentary rocks having hematite concretion cement in case of MB. The laminations in the host rock of MB are not disrupted. In contrast, the ‘fluid pathways’ cut across the concentric layering of the VHC.

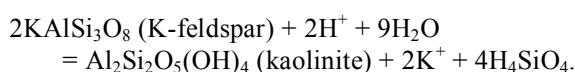
The inherent porosity and permeability of the host sandstone facilitate movement of large volumes of fluid

through it in the VHC. The red streaks are distinctly heavy mineral-lined foreset laminae of the arenite beds. The red colouration is possibly due to oxidation of iron-oxide bearing silicate or sulphide minerals. This reddening could be related to present-day supergene weathering as well. The fluid was iron-rich as evidenced by the occurrence of thin, millimetre-scale, iron-rich streaks in the host sandstone running nearly parallel to bedding (Figure 3 c). These streaks warp around the hematite-rich concretions in their outer part, cut across the concretionary layering while moving parallel to relict primary sedimentary structure preserved in the inner part. This is identical to the layering geometries inside and outside the concretions shown by Sellés-Martínez¹², suggesting syn-compactional origin of selvages (Figure 3 d) related to diagenesis. The conformity of these streaks with the primary sedimentary structures within the concretion clearly indicates the growth of the concretions on pre-existing structures. However, the warping of the streaks around the concretions also suggests that they were impervious and forced the fluid flow paths around them. The outcrop scale evidence of possible fluid pathways in the Bihariya area is quite significant since it demonstrates the transportation of iron-rich fluid to the site of concretion formation (Figure 3 c). When a fluid, of reducing nature mixes with oxidizing groundwater, iron precipitates as hematite and/or goethite cement at the mixing front^{4,19,20}.

In addition, the nucleus (presently clay-rich after k-feldspar) in itself can act as an oxidant in a solution mix. Because the fluid pathways present within and around the hematite concretion are distinct and the iron-rich traces clearly depict the selective precipitation of iron in the cap portion of the concretion and in the fringes. The Kaolinitic nuclei within the hematite concretions can be explained by the alteration of minor K-feldspar in the sediment to kaolinite, which in turn would have provided sites for the growth of concretions by selectively removing Fe from the solution. In a solution with high Fe/Al, the ferrous Fe in solution can be locally oxidized to Fe³⁺, which replaces for Al³⁺ in kaolinite producing Fe-kaolinite. These Fe-kaolinite clusters would have served as preferred sites for the formation of concretions later during general oxidation of the reduced groundwater that conveyed the dissolved iron as Fe²⁺. Also in the initial stage, a feedback mechanism would have promoted the sequestration of Fe in these isolated centres as the oxidation of Fe would have given rise to local low-pH conditions that helped further alteration of K-feldspar to kaolinite and perhaps its complete elimination. While the formation of kaolinite is accompanied by the removal of SiO₂ as H₄SiO₄ in solution on a local scale, widespread dissolution of quartz would have occurred during general oxidation accompanying the growth of hematite concretions leading to the now-observed friability of the host sandstone. The formation of hematite due to oxidation of ferrous iron in the presence of water makes the environment acidic according to the following reaction



The formation of kaolinite from K-feldspar can be represented by the reaction



The hematite-rich concretions of the Bihariya area show multiple iron-rich layers separated by iron-poor layers with a distinct nucleus. The presence of a nucleus and zonation are common in concretions⁴. It is clear that the physico-chemical condition existing at the oxic–anoxic boundary at in the site of concretion formation was dynamic in time and space. The introduction of multiple fluid phases to create an oxic–anoxic interface for concretion formation was proposed⁴, since the concretions lacked a nucleus. Otherwise, the nucleus could have acted as an oxidant for the formation of hematite from the iron-rich fluid phase passing through the host arenite. The clay-rich cores and rims observed in Bihariya hematite concretions possibly can give rise to different Fe-rich layers. The nucleus is possibly shielded after the formation of each layer so that the core can further act as an oxidation front for the outer layers to develop in space and time.

Conclusion

The hematite-rich VHC concretions formed during diagenetic process are broadly similar to MB and other reported terrestrial analogues from different parts of the world in terms of their morphology, mineralogy, spectral signatures and host-rock characteristics. The differences between MC and UC are well known. Similarly, the VHC structures show subtle differences in terms of their occurrence in an older lithological horizon and distinct presence of a nucleus. UC samples are reported from Jurassic Navajo Sandstone and the VHC structures are observed in Mesoproterozoic Dhandraul Sandstone. However, the respective ages of concretion formation are still unknown. Experimental and numerical simulation studies have suggested that ‘blueberries’-like concretion development requires a nucleus⁵, and the multi-rimmed VHC samples are nucleus-bearing unlike MC and UC structures. However, the presence of hematite in the VHC is similar to that MC and UC, and this has been verified by various analytical techniques. The outcrop evidence showing distinct traces of possible fluid pathways provides further proof for the role of water in the concretion formation. In the absence of return samples, the study of various Martian analogues from multiple locations worldwide occurring in diverse geological settings is crucial to understand the past geological processes of the ‘wet’ red planet.

1. Squyres, S. W. *et al.*, *In situ* evidence for an ancient aqueous environment at Meridiani Planum, Mars. *Science*, 2004, **306**, 1709–1714.
2. Chan, M. A., Beitler, B., Parry, W. T., Ormö, J. and Komatsu, G., A possible terrestrial analogue for hematite concretions on Mars. *Nature*, 2004, **429**, 731–734.
3. Ormö, J., Komatsu, G., Chan, M. A., Beitler, B. and Parry, W. T., Geological features indicative of processes related to the hematite formation in Meridiani Planum and Aram Chaos, Mars: A comparison with diagenetic hematite deposits in southern Utah, USA. *Icarus*, 2004, **171**, 295–316; doi:10.1016/j.icarus.2004.06.001.
4. Chan, M. A., Beitler, B. B., Parry, W. T., Ormö, J. and Komatsu, G., Red rock and red planet diagenesis: comparisons of Earth and Mars concretions. *GSA Today*, 2005, **15**(8), 4–10.
5. Chan, M. A., Ormö, J., Park, A. J., Stich, M., Souza-Egipsy, V. and Komatsu, G., Models of iron oxide concretion formation: field, numerical, and laboratory comparisons. *Geofluids*, 2007, **7**, 356–368.
6. Benison, K. C., A Martian analog in Kansas: comparing Martian strata with Permian acid saline lake deposits. *Geology*, 2006, **34**, 385–388.
7. Benison, K. C. and Bowen, B. B., Acid saline lake systems give clues about past environments and the search for life on Mars. *Icarus*, 2006, **183**, 225–229.
8. Bowen, B. B., Benison, K. C., Oboh-Ikuenobe, F. E., Story, S. and Mormile, M. R., Active hematite concretion formation in modern acid saline lake sediments, Lake Brown, Western Australia. *Earth Planet. Sci. Lett.*, 2008, **268**, 52–63.
9. Morris, R. V. *et al.*, Hematite spherules in basaltic tephra altered under aqueous, acid-sulfate conditions on Mauna Kea volcano, Hawaii: possible clues for the occurrence of hematite-rich spherules

- in the Burns formation at Meridiani Planum, Mars. *Earth Planet. Sci. Lett.*, 2005, **240**, 168–178.
10. Glotch, T. D., Christensen, P. R. and Sharp, T. G., Fresnel modeling of hematite crystal surfaces and application to Martian hematite spherules. *Icarus*, 2006, **181**, 408–418.
 11. Bowen, B. B., Benison, K. C., Oboh-Ikuenobe, F. E., Story, S. and Mormile, M. R., Active hematite concretion formation in modern acid saline lake sediments, Lake Brown, Western Australia. *Earth Planet. Sci. Lett.*, 2008, **268**, 52–63.
 12. Sellés-Martínez, J., Concretion morphology, classification and genesis. *J. Earth Sci. Rev.*, 1996, **41**, 177–210.
 13. Catling, C., On Earth, as it is on Mars? *Nature*, 2004, **429**, 707–708; doi:10.1038/429707a.
 14. Kumar, A., Kumari, P., Dayal, A. M., Murthy, D. S. N. and Gopalan, K., Rb–Sr ages of Proterozoic kimberlites of India: evidence for contemporaneous emplacements. *Precambrian Res.*, 1993, **62**, 227–237.
 15. Rai, P. and Pati, J. K., High temperature and atmospheric pressure study of silica sand (\pm Na₂CO₃) from Sankargarh area, Allahabad district and its implications. *Indian J. Geochem.*, 2003, **18**, 49–54.
 16. Chakraborty, C., Sedimentary records of Erg development over a braidplain: Proterozoic Dhandraul Sandstone, Vindhyan Supergroup, Son Valley. In *Recent Advances in Vindhyan Geology* (ed. Bhattacharyya, A.), Memoir Geological Society of India, 1996, vol. 36, pp. 77–99.
 17. Pati, J. K., Malviya, V. P. and Prakash, K., Basement reactivation and its relation to neotectonic activity in and around Allahabad, Ganga plain. *J. Indian Soc. Remote Sensing*, 2006, **34**, 47–56.
 18. Chevrier, V., Roy, R., Le, M. S., Borscheneck, D., Mathé, P. E. and Rochette, P., Spectral characterization of weathering products of elemental iron in a Martian atmosphere: implications for Mars hyperspectral studies. *Planet. Space Sci.*, 2006, **54**, 1034–1045.
 19. Berner, R. A., Goethite stability and the origin of red beds. *Geochim. Cosmochim. Acta*, 1969, **33**, 267–273.
 20. Von Gunten, U. and Schneider, W., Primary products of oxygenation of iron (II) at an oxic/anoxic boundary; nucleation, agglomeration, and aging. *J. Colloid Interface Sci.*, 1991, **145**, 127–139.

ACKNOWLEDGEMENT. We thank the anonymous reviewer for his valuable suggestions that helped improve the manuscript.

Received 8 December 2014; revised accepted 22 March 2016

doi: 10.18520/cs/v111/i3/535-542